TITLE

Pinwheel-dipole configuration in cat early visual cortex

RUNNING HEAD

Pinwheel-dipole configuration in cat visual cortex

AUTHORS

Jérôme Ribot[1,†,*], Alberto Romagnoni[1,†], Chantal Milleret[2], Daniel Bennequin[3,‡], Jonathan Touboul[1,4,‡]

AFFILIATIONS

[1]Mathematical Neuroscience Team, CIRB - Collège de France (CNRS UMR 7241, INSERM U1050, UPMC ED 158, MEMOLIFE PSL), 11 Place Marcelin Berthelot, 75005 Paris

[2]Spatial memory and navigation team, CIRB - Collège de France (CNRS UMR 7241, INSERM U1050, UPMC ED 158, MEMOLIFE PSL), 11 Place Marcelin Berthelot, 75005 Paris

[3]Géométrie et dynamique, Université Paris Diderot (Paris VII), Paris, France

[4]INRIA Mycenae Team, Paris-Rocquencourt, France.

[*]Correspondence to: jerome.ribot@college-de-france.fr

[†,‡]Equal contribution

ABSTRACT

In the early visual cortex, information is processed within functional maps whose layout is thought to underlie visual perception. However, the precise organization of these functional maps as well as their interrelationships remains unresolved. Here, we show that spatial frequency representation in cat areas 17 and 18 exhibits singularities around which the map organizes like an electric dipole potential. These singularities are precisely co-located with singularities of the orientation map: the pinwheel centers. We first show, using high resolution optical imaging, that a large majority (around 80%) of pinwheel centers exhibit in their neighborhood semi-global extrema in the spatial frequency map. These extrema created a sharp gradient that was confirmed with electrophysiological recordings. Based on an analogy with electromagnetism, a mathematical model of a dipolar structure is proposed, that was accurately fitted to optical imaging data for two third of pinwheel centers with semi-global extrema. We conclude that more than half of orientation pinwheel centers form spatial frequency dipoles in cat early visual cortex. Given the functional specificities of neurons at singularities in the visual cortex, it is argued that the dipolar organization of spatial frequency around pinwheel centers could be fundamental for visual processing.

KEY WORDS

Cortical maps; Dipole; Orientation; Singularities; Spatial frequency

INTRODUCTION

The brain contains the representations of multiple sensory features that form continuous and orderly maps. These maps subtend perception, yet the principles governing their organization remain fundamentally unknown. Uncovering the fine structure of maps can reveal their underlying organizing principles and shed new light on how the brain processes the sensory information.

The early visual cortex (V1 and V2) of higher mammals provides a particularly appropriate cortical area to investigate these questions. Its neurons are selective locally to several attributes of the visual scene, such as the orientation (OR) of a stimulus (Hubel & Wiesel, 1959) and its spatial frequency (SF) (Movshon et al., 1978). Neurons with similar functional properties are clustered vertically and form functional maps parallel to the cortical surface. The organization of the OR map has been extensively studied in the past 20 years: it consists of regular zones where preferred OR varies smoothly, together with singularities, the *pinwheel centers* (PCs), in the vicinity of which all ORs are represented (Fig. 1A, black circles) (Bonhoeffer & Grinvald, 1991).

In contrast, the organization of the SF map has been the subject of a long-standing debate. A common view is that its layout should be constrained to that of the OR map in order to enhance uniform coverage (i.e., even representation of all combinations of the attributes, Swidale et al, 2000). This view is supported by several experiments showing that lines of iso-properties tend to run perpendicular to each other (Yu et al., 2005; Nauhaus et al., 2012), but also that OR PCs are situated preferentially at local SF extrema (Shoham et al., 1997; Issa et al, 2000; Issa et al., 2008).

On the other hand, it was recently argued that the latter discovery may result from using high-pass filtering methods that lead to the over-representation of extreme SF values at PC locations (Ribot et al., 2013). Instead, our own data using new techniques for intrinsic optical imaging (Kalatsky & Stryker, 2003) have suggested that signal-to-noise ratio is weak near PCs, making it very hard to extract SF preference, even more so since both OR and SF gradients seem sharp in these *indeterminacy* regions (Ohki et al., 2006; Ribot et al., 2013). Eventually, PCs were proposed to be common organizers of the two maps, with iso-OR and iso-SF lines that tended to be parallel to each other rather than orthogonal, violating the concept of uniform coverage.

In this study, we focused on these particular locations in the OR map in order to reveal their precise SF structure. We used high-resolution intrinsic optical imaging in cat visual cortex (A17 and A18) to show that a majority of PCs had a stereotyped dipolar structure in the SF map. This dipolar structure created an abrupt, discontinuous change in SF representation when pinwheel was crossed, which was confirmed with targeted multi-units recordings. The functional role of this pinwheel-dipole configuration is discussed and it is proposed that representing a large range of SFs close to PCs is beneficial for visual perception.

MATERIALS AND METHODS

Five adult cats (two males, three females), aged between 24 and 72 weeks and born from different litters in our colony, were studied. They were all in good health and had no apparent malformations or pathologies. All experiments were performed in accordance with the relevant institutional and national guidelines and regulations i.e. those of the Collège de France, the CNRS and the DDPP (JO 87-848, consolidated after revision on May 30, 2001, Certificate n° 75-1754, French "Ministère de l'Agriculture et de la Pêche"). They also conformed to the relevant regulatory standards recommended by the European Community Directive (Directive 2010/63/UE) and the US National Institutes of Health Guidelines.

Surgical procedure

On the day of the optical imaging experiment, animals were anaesthetized with Saffan® (initial, i.m., 1.2 mg/Kg; supplements, 1:1 in saline, i.v. as needed). After tracheal and venous cannulation, electrocardiogram, temperature and expired CO_2 probes were placed for continuous monitoring. Animals were installed in a Horsley-Clarke stereotaxic frame and prepared for acute recordings. The scalp was incised in the sagittal plane, and a large craniotomy was performed overlying areas 17 and 18 of both hemispheres. The nictitating membranes were then retracted with eye drops (Neosynephrine® 5%, Ciba Vision Ophthalmics, France) and the pupils dilated with atropine eye drops (Atropine 1%, MSD-Chibret, France). Scleral lenses were placed to protect the cornea and focus the eyes on a tangent screen at a distance of 28.5 cm. The size of the lenses was adapted to the eye of each cat. Animals were then paralyzed with an infusion of Pavulon (0.2 ml/kg, i.e., 0.4 mg/kg i.v.) and breathing was assisted artificially through a tracheal cannula with a 3:2 mixture of N_2O and O_2 containing 0.5–

1.0% isoflurane. The respiration frequency was adjusted to around 18 per minute and the volume adapted to the ratio of exhaled CO_2 (pCO_2 was maintained at 4%). Paralysis was maintained throughout the recording by continuous infusion of a mixture of Pavulon (0.1 ml/kg/h) diluted in glucose (5%) and NaCl (0.9 g/l). At the end of the recording session, the animal was given a lethal dose of pentobarbital. The experiments lasted less than 12 hours.

Optical imaging

The cortex was illuminated at 545 nm to reveal the vascular pattern of the cortical surface and at 700 nm to record the intrinsic signals. The focal plane was adjusted to 500 µm below the cortical surface. The optic discs were plotted by tapetal reflection on a sheet of paper covering the tangent screen. The centre of the screen was situated 8 cm (~15°) below the middle of the two optic discs, that is, ~8.5° into the lower visual field (Bishop et al., 1962). Intrinsic optical signals were recorded while the animal was exposed to visual stimuli displayed on a CRT monitor. The size of the display subtended a visual angle of ~75° x 56°. The image had a resolution of 14 pixels per degree and the refresh rate was 88 Hz. Frames were acquired by CCD video camera (1M60, Dalsa, Colorado Springs, USA) at the rate of 40 frames per second and were stored after binning by 2 x 2 pixels spatially and by 12 frames temporally using the LongDaq system (Optical Imaging Inc., New York, USA). In three animals, images were acquired at a resolution of approximately 15.3 µm/pixel via a 50x50 mm tandem lens configuration. To illustrate the fine representation of SF around OR pinwheel centre (Fig. 1 and 2 of the main text), a 135x50 mm configuration was used to reach a spatial resolution of 5.9 µm/pixel.

Stimulation

Full-screen visual stimuli were presented continuously to the animal. Each stimulus consisted of sine-wave gratings drifting in one direction and rotating in a counter-clockwise manner (Kalatsky & Stryker, 2003). The angular speed of the rotation was 2 rotations per min. The temporal frequency of the drift was 2 Hz. The contrast was set at 50%. Thirty SFs ranging linearly in a logarithmic scale from 0.039 to 3.043 cycle/degree (cpd) were presented in random order. Ten full rotations were presented for each SF. At the end of the last rotation, the first frame of the first rotation for the next SF was presented without interruption. The total duration of the recording was 2.5 hours.

When optical imaging was combined with multi-unit recordings, two SFs of 0.15 cpd and 0.68 cpd were used to reduce the duration of the recording (10 minutes) and of the *off-line* analysis.

Image processing

Data analysis was based on the method developed by Kalatsky and Stryker (2003) to extract periodic signals from intrinsic data in Fourier space. First, data were pre-processed with the generalized indicator function method (Yokoo et al., 2001; Ribot et al., 2006). This procedure was applied to raw data for each SF separately. A low-pass filter with a Gaussian kernel of around 15 μm half width was also applied for smoothing the data.

To construct the OR map, a Fourier transform was performed on the temporal signal of each pixel for all SFs together. The phase at the frequency of rotation was calculated to

obtain the preferred OR (plus the hemodynamic delay) at each pixel (Kalatsky and Stryker, 2003). The hemodynamic delay (approximately 2.5 s) was subtracted from all OR maps.

Then intrinsic signals related to each SF were considered separately. For each pixel, the modulation of the signal induced by the rotation of the gratings was interpolated via a least-square method with a cosine function whose phase was equal to the preferred OR at this pixel and whose frequency was equal to half the frequency of rotation. As a result, magnitude maps for preferred ORs were obtained for each stimulus SF. These maps are referred as "maximal intensity maps". Pixels with negative values, which corresponded to interpolation peaking at orthogonal ORs, were rectified to zero. Then, values were rescaled for each pixel by setting the greatest value among all SFs to 100 (Fig. S1).

Finally, the location of the functional border between A17 and A18 was estimated based on the difference between the maximal intensity maps at 0.15 cpd and 0.5 cpd (Bonhoeffer et al., 1995; Ohki et al., 2000).

Determining the preferred spatial frequency

To determine the preferred SF at each pixel, the intrinsic signals were interpolated with a difference of Gaussians (DOG) function:

$$DOG(SF_{stim}) = A_1 \exp(\frac{SF_{stim}^{\ 2}}{2\sigma_1^{\ 2}}) - A_2 \exp(\frac{SF_{stim}^{\ 2}}{2\sigma_2^{\ 2}}) \quad (1)$$

where SF_{stim} represents the SF of stimulation, A_1 and A_2 are the amplitude of each Gaussian function, and σ_1 and σ_2 are related to the bandwidth of each Gaussian

function. Values for A_1, A_2, σ_1 and σ_2 were optimized to provide a least square error fit to the data using Matlab®.

At each pixel, the error-of-fit was defined by

$$\left(\frac{\sum_{SF_{stim}} \left[S(SF_{stim}) - DOG(SF_{stim}) \right]^2}{\sum_{SF_{stim}} \left[S(SF_{stim})^2 + DOG(SF_{stim})^2 \right]} \right)^{1/2} \qquad (2)$$

where $S(SF_{stim})$ represents the values of the intrinsic signal for the SF of stimulation. It ranged between 0 (perfect fit) and 1 (worst fit). Pixels with an error-of-fit greater than 0.5 were discarded from further analysis (Ribot et al., 2013).

Two parameters were extracted from this interpolation: the preferred SF, which is the SF corresponding to the peak of the tuning curve, and the "full-width at half-height" (FWHH), defined as the ratio between the highest and lowest frequencies to which the pixel was at least half as responsive as it was to its preferred SF. The latter parameter was expressed in octaves.

Existence of a local maximum and/or a minimum in the SF map

In order to check whether the SF representation around pinwheels exhibited a maximum and/or a minimum, pinwheel locations were first automatically determined from the OR map. A region of interest was then set 150 µm around each pinwheel, as in Fig. 1 of the main text. The pinwheels with overlapping regions of interest were rejected since this could cause a mutual interference in SF representation.

As shown in Fig. 1 of the main text, the indeterminacy zone for SF (with an error-of-fit >0.5) could additionally vary from pinwheel to pinwheel. In order to ensure accurate estimates of the SF representation, we considered only pinwheels whose

indeterminate zone covered less than 75% of the total area of interest. This corresponded to 115 PCs in A17 and 109 PCs in A18.

A pixel in the SF map was defined as a maximum (or minimum) if its value belonged to the upper (or lower) third of the SF values calculated over a hypercolumn: Following our previous results (Ribot et al., 2013), the SF structure in A17 is quasi-periodic, with periods ranging between 0.79 mm in the mediolateral direction and 1.43 mm in the anteroposterior direction. We estimated here a hypercolumn as a circle of 1.11 mm diameter (i.e. the average of the two values). In A18, the diameter of a hypercolumn was set to 1.5 mm (Ribot et al., 2013).

Fitting the dipolar model

Equation (3) was fitted via a least-square method to the experimental data for those PCs having a local maximum and a local minimum in their neighborhood. For each fit, the coefficient of determination R^2 was calculated using the Matlab® function *regress* in order to have information on the goodness of fit of the model. Only those fit with $R^2 > 0.8$ (i.e. fits for which 80% in the response variable can be explained) were kept in order to provide biologically relevant parameters in Fig. 6.

Electrophysiology

In order to confirm abrupt changes of SF representation around pinwheel centers, we made targeted multi-unit recordings using the NeuraLynx system after off-line analysis of optical imaging data. Tungsten microelectrodes (1–2 MΩ at 1 kHz) were used. The electrical signal was amplified and band-pass filtered between 0.3 and 3 kHz. Then, unit responses were thresholded with a window discriminator to separate spike

activity from electrical noise.

The average depth from cortical surface for the first recording was 325 ± 65 μm s.d. across the four penetrations. Sine-wave gratings of different ORs (n=8) were presented randomly to the animal. The gratings, with a SF of 0.37 cpd, drifted perpendicularly to the OR at a temporal frequency of 2 Hz. Sixteen directions were presented 20 times to the animal for a period of 1 s each, interleaved by blank-screen stimuli for 1 s in order to provide measures of spontaneous activity.

Once OR preference was determined, subsequent stimuli consisted of pseudo-randomly ordered sine-wave gratings spanning a logarithmic range of SFs between 0.08 and 1.23 cpd (10 SFs in total, with 0.44 octave increments). The gratings were presented at the preferred OR, and 30 trials were presented for each stimulus. Blank-screen stimuli were presented for 1 s interleaved with grating stimuli to measure spontaneous activity. This spontaneous activity was subtracted from the activity evoked by each SF. Five recordings were made for each penetration at regular intervals of 100 μm. The average depth of the deepest recording was 725 ± 65 μm s.d. among the four penetrations. Then, spike activity was summed up among the five depths to obtain an estimate of the SF response of the population of neurons at each targeted location.

RESULTS

Figure 1

Spatial Frequency representation near Orientation Pinwheel Centers

A detail of OR and SF maps obtained with these experimental and image processing techniques is shown in Fig. 1 (see also Fig. S1). Four PCs are selected in A17 to illustrate the SF structure at these locations (Fig. 1A-B, black circles). The activity induced by the stimulation with various SFs within a 150 μm radius of PC 1 is shown in Fig. 1C. The immediate neighborhood of the PC is activated by a broad range of SFs. As the stimulus SF is increased, the activity, initially restricted to the lateral part of the PC, gradually invades the whole cortical area and almost completely fills it for SFs between 0.4 to 0.6 cpd. It then decays on the lateral part of the PC, while higher activity remains on the medial part above 0.9 cpd. There were no responses for SFs larger than 2 cpd. As a consequence, preferred SF representation shows spatial variations winding around the PC with local minimum (low SF) in the lateral part opposite to a local maximum (high SF) in the medial part (Fig. 1D1).

This structure constitutes a singularity in the SF map, co-localized with the PC. The SF structure for PCs 2 to 4 is shown in Fig. 1D2-4. PCs 2 and 3 also exhibit maximum and minimum values separated by around 2.5 octaves. But while the extrema are aligned with PC 2, they are close to orthogonal in PC 3. The SF map of PC 4 has a clear maximum on one side of the PC, but no SF as low as for the three others on the other side of the PC. But it still displays a singularity, as indicated by the sharp transition in SF levels.

Figure 2

Existence of a local maximum and/or a minimum in the SF map around PCs

Extreme SF values therefore seem to be represented near PCs. In order to check this, a region of interest was then set 150 µm around each PC. A pixel in this region of interest was then defined as a maximum (or minimum) if its value belonged to the upper (or lower) third of the SF values calculated over a hypercolumn around the PC (see Methods).

Figures 2D and 2E illustrates this process for the two PCs shown in Fig. 2A-C. Top panels show the distribution of preferred SFs within 150 µm from the two PCs (Fig. 2A-C, red circles). Below is shown the distribution of preferred SFs within a hypercolumn (Fig. 2B-C, black circles). With our criteria, the first PC exhibited both a local maximum and a local minimum. On the other hand, the second PC only had a local maximum.

A quantitative analysis (Fig. 2E and 2F) shows that 89.6% (103/115) of the PCs in A17 and 76.2% (83/109) in A18 present the two semi-global extrema within 150µm. Other PCs only display one extremum. It is thus concluded that extreme SFs are represented near PCs.

Figure 3

Electrophysiological confirmation of the abrupt change in SF representation

The abrupt change in SF representation at PCs induced by these extreme values was confirmed with targeted, multi-unit recordings (Fig. 2A-B, white dots) in superficial layers. While preferred orientation estimated most superficially (Fig. 2C) matches the one calculated with optical imaging, the SF tuning exhibited fluctuations among the different

depths (Fig. 2D, thin lines). This possibly reflects the weak clustering of neurons for SF found in a previous study (DeAngelis et al., 1999). But the averaged activity (thick line) confirms the abrupt variation in preferred SF observed with optical imaging (Fig. 2B). Locations 1 and 2 prefer SFs lower than 0.2 cpd. Location 3 (within 100 μm of the PC) yields maximal response between 0.37 and 0.68 cpd (Fig. 2D3). On the other side of the PC (location 4), peak response is for 0.68 cpd.

Figure 4

Geometrical description of a Pinwheel-Dipole

These properties suggest that the organization of SF around PCs in cat is highly non-orthogonal to the OR map. SF representation is rather analogous to the *dipolar architecture* displayed, for instance, by the electric potential created by an electric dipole. In order to ensure that the SF representation near PCs is indeed dipolar, we propose here an analytic model for fitting SF representation around those PCs having both a maximum and a minimum within 150 μm.

For this purpose, we considered a circular region of radius $R = 150\ \mu m$ (the pinwheel area, PA) around a PC. Classical neuro-geometrical theory (Petitot, 2008) describes the OR map in the PA as the half angle of a complex coordinate $z = r.\exp(i.\varphi)$ (Fig. 3A,B), defined modulo π:

$$\theta(r,\varphi) = \frac{\varphi}{2} + \varphi_0\ ,$$

where φ_0 is an arbitrary phase depending on the pinwheel considered.

As for an ideal model of dipolar topology, we shall use the classical shape of the two-dimensional electric potential created by an electric dipole, which is known to physicists to be proportional to the inverse of the distance from the center of the dipole. A simple, idealized map displaying dipolar architecture in the PA can thus be described as:

$$\nu(\mathrm{r},\varphi) = \mathrm{Re}\left(\frac{R}{z}\right) = \frac{R}{\mathrm{r}}\cos\varphi\ .$$

This function exhibits a singularity at the PC (*z=0*) where it reaches both its minimal and maximal value and shows symmetrical circular level sets 180° apart from the singularity.

In order to fit this function with optical imaging data, we allowed deformations of this idealized model. The geometrical model of the SF map structure in the PA is defined as follows:

$$\nu_{dip}(\mathrm{r},\varphi) = A.\frac{R}{\mathrm{r}\sqrt{(\cos\psi)^2\,(\cos\varphi)^2\ +\ (\sin\psi)^2\,(\sin\varphi)^2}}\cos\tilde{\varphi} + h_0, \qquad (3)$$

where $\tilde{\varphi}$ is an angular deformation allowing architectures in which circular level sets are not 180° apart:

$$\tilde{\varphi} = \varphi + 2\pi\,\gamma\ \cos\varphi$$

In addition, we considered equation (3) saturating at the maximum and minimum SF values ν_{max} and ν_{min}. This saturation allows consistency with the experimental data by avoiding the divergence of ν_{dip} at the singularity.

Figure 4C-G display the architecture of these maps for different representative values of ψ, γ, h_0 and A. The variation of these parameters allows continuous deformations of the shape of the iso-SF lines. It is important to notice, however, that the topology of the level sets remains unchanged.

Figure 5

Fitting optical imaging data

Figure 5 shows an example of fit with equation (3) in a region of interest covering A17 and A18. Only those PCs for which both a SF semi-global maximum and minimum could be detected in the PA, and for which the zone of SF indetermination was smaller than 75%, were fitted (white circles in Fig. 4A and 4B). These PCs are numbered with decreasing coefficient of determination following the fit. A larger view of the SF representation around those PCs is shown in Fig. 5C, top rows. SF representation was rescaled so that red and blue colors corresponded to the local maximum and minimum of each PC, respectively. The fit with equation (3) is shown below by optimizing in each case the scalar parameters $\psi, \gamma, h_0, A, \nu_{min}$ and ν_{max}.

Among the 186 PCs tested, we found that around two third of the fits had a coefficient of determination R^2 greater than 0.8 (Fig. 4D, 123/186=66.1 %), i.e. that 80% of the variations could be captured by the model. Fits with R^2 less than 0.8 typically corresponded to complex SF representation with multiple minima and/or extrema. No difference could be found between A17 (68/103=66.0%) and A18 (55/83=66.3%). We therefore conclude that a majority of PCs in the two visual areas have a dipolar SF organization.

Figure 6

Statistics of the fits

Figure 6 shows the distribution of the parameters in equation (3) that were obtained from the fits over the 123 PCs with R^2 greater than 0.8. This led to a robust estimate of each parameter in the model.

First we evaluated how the difference between the local SF extrema $\nu_{max} - \nu_{min}$ was distributed among the PCs. For this purpose, $\nu_{max} - \nu_{min}$ was plotted with respect to the percentage of SF indetermination (Fig. 6A). We found that the difference $\nu_{max} - \nu_{min}$ decreased with the percentage of SF indetermination (slope of -1.67) and crossed the ordinate axis for 2.28 octaves. This suggests that extreme SF values tend to be hidden when the zone of indeterminacy is large. This is consistent with the idealized dipole model that locates extrema at the singularity: the smaller the indeterminacy area, the larger the SF range. Eventually, we conclude that the mean (± sd) value for $\nu_{max} - \nu_{min}$ in equation (3) is 2.28 ± 0.81 octaves.

Then, the DC component h_0 was plotted with respect to the average value between ν_{max} and ν_{min} (Fig. 6B). We found a noticeable correlation between the two parameters (slope 0.99). An estimate (± sd) of the coefficient h_0 in equation (3) is thus $\frac{\nu_{max}+\nu_{min}}{2}$ ± 0.37 octaves.

Figure 6C shows the angle difference between the two extrema, which is related to the parameter γ in equation (3) (see Figure 4E for example). Surprisingly, we found that this angle was biased toward the highest values, indicating that the location of the maximum and

the location of the minimum are preferentially located symmetrically with respect to the PC. Variations however existed, for which the sd was evaluated to 56 degrees.

Finally, we evaluated the values of the parameters ψ and A. The mean (± sd) value for the slope ψ was 0.7 (± 0.37) radians (Fig. 6D), i.e. close to π/4 for which no additional deformation occurs. The parameter A was estimated by plotting its values with respect to $(\nu_{max} - \nu_{min})/2$ (Fig. 6E). We found a positive correlation between these two parameters (slope = 0.44). An estimate (± sd) of the parameter A is thus $0.44 * \frac{\nu_{max}-\nu_{min}}{2} \pm 0.37$ octave.

The resulting dipole for the average values of the parameters h_0, γ, ψ and A is the dipole represented in Fig. 4C.

DISCUSSION

These results thus shed new light on the structure of cortical maps in cat early visual cortex. We show that singularities in the OR map form dipoles in the SF map for at least 54.9% (123/224) of the PCs tested in A17 and A18. Other PCs couldn't be accurately fitted with the dipolar model we proposed (63/224=28.1%) or did not have simultaneously a maximum and a minimum in their neighborhood (38/224=17%). Even in the latter case, however, SF discontinuity can still occur at pinwheel singularities (See Fig. 1D4 for instance), with a single extremum located close to the PC but not at the center of it.

Dipoles and uniform coverage

The SF dipoles create discontinuities in SF representation as the OR PCs create sharp gradients in the OR map. This result is reminiscent of early investigations by Das and Gilbert (1997) of the relationships between the map of visual space and the orientation map: These authors showed that the map of visual space had local distortions that also registered with OR PCs. Although these results were thereafter disputed (Hetherington & Swindale, 1999; Buzás et al., 2003), they raised fundamental questions about how multiple cortical maps should be represented on a single cortical sheet.

At the present time, the dominant theory proposes that continuity and coverage uniformity constitute fundamental principles governing the organization of these maps (Swindale 1991; Swindale et al., 2000). However, the dipolar structure reported here does not allow uniform coverage, since a specific range of ORs is represented for a specific range of SFs. On the other hand, the dipole ensures the representation of a large range of SFs in the immediate neighborhood of the singularity, as the pinwheel does in the OR map. As shown in a companion paper (Romagnoni et al., 2014), pinwheel-dipole singularities may instead

enhance the balanced detection of OR and SF, which would not be possible under the uniform coverage hypothesis.

Dependence between orientation and spatial frequency representations

The striking co-localization of OR PCs and SF dipoles likely emerges from developmental constraints. Indeed, immature OR maps exist early after eye opening (Crair et al., 1998) at a time when only low SFs are represented (Tani et al., 2012). Afterwards, both maps jointly develop with visual experience (Tani et al., 2012). Such interdependence of the two features is also reflected by the variations of preferred SF with stimulus OR (Webster & De Valois, 1985; Issa et al, 2000), and by the response to complex stimuli when varying SF, speed and direction (Basole et al., 2003). We conclude that OR and SF are not independently represented in cat primary visual cortex, and therefore should be studied jointly.

Whether this dependence between maps is also true for other mammals, including humans, however remains undetermined. It would not be surprising if different species adopted distinct coding strategies adapted to the number of features encoded in the primary visual cortex and to their specific circuit organization. For instance, maps of preferred OR and SF in the primate tend to show sharp orthogonality (Nauhaus et al., 2012), which is not the case of ferrets (Yu et al., 2005). However, these global statistics on the whole maps shall be finely studied near PCs to uncover SF representation at these locations.

Exhaustivity and parsimony at pinwheel-dipole centers

Pinwheel and dipole structures have fascinating and universal geometric features. As shown in the companion paper (Romagnoni et al., 2014), the pinwheel is the unique continuous architecture ensuring exhaustive representation of a periodic quantity with minimal

redundancy. Similarly, the dipole is the most parsimonious continuous topology ensuring a local representation of a non-periodic open range of SF values. Both topologies thus allow collecting economically all information, which could be fundamental for visual processing. In particular, neurons at PCs have been shown to exhibit properties distinct from those in the regular domains: they show strong resistance to monocular deprivation (Crair et al., 1997), are maximally sensitive to OR adaptation (Dragoi et al., 2001) and have a high dynamical variability (Schummers et al., 2002). They also receive intracortical inputs from domains signaling a wider range of ORs (Yousef et al., 2001, Schummers et al. 2002). Properties related to SF perception at pinwheel-dipole centers, such as enhanced SF adaptation (Sharpee et al., 2006) or their interactions with nearby cortical regions, could exhibit similar specificities, and, for these purposes, collecting a large range of SFs would be beneficial.

REFERENCES

Basole, A., White, L.E. & Fitzpatrick, D. (2003) Mapping multiple features in the population response of visual cortex. Nature 423:986 –990

Bishop, P.O., Kozak, W. & Vakkur, G.J. (1962) Some quantitative aspects of the cat's eye: axis and plane of reference, visual field co-ordinates and optics. J Physiol 163:466 – 502.

Bonhoeffer T., Kim D.S., Malonek D., Shoham D. & Grinvald A. (1995) Optical imaging of the layout of functional domains in area 17 and across the area 17/18 border in cat visual cortex. Eur J Neurosci., 7:1973–1988.

Buzás P., Volgushev M., Eysel U.T. & Kisvarday Z.F. (2003) Independence of visuotopic representation and orientation map in the visual cortex of cat. Eur J Neurosci., 18 :957-968

Crair, M.C, Ruthazer, E.S, Gillespie, D.C. & Stryker, M.P. (1997) Relationship between the ocular dominance and orientation maps in visual cortex of monocularly deprived cats. Neuron. 19(2):307-18.

Crair, M.C, Gillespie, D.C & Stryker, M.P. (1998) The role of visual experience in the development of columns in cat visual cortex. Science. 279(5350):566-70.

DeAngelis, G.C., Ghose, G.M., Ohzawa, I. & Freeman, R.D. (1999) Functional micro-organization of primary visual cortex: receptive field analysis of nearby neurons. J Neurosci 19:4046–4064.

Dragoi, V., Rivadulla, C. & Sur, M. (2001) Foci of orientation plasticity in visual cortex. Nature. 411(6833):80-6.

Hetherington P.A. & Swindale N.V. (1999) Receptive field and orientation scatter studied by recordings in cat area 17. Visual Neuroscience. 16 :637-652

Hubel, D.H. & Wiesel, T.N. (1959) Receptive fields of single neurones in the cat's striate cortex. J. Physiol. 148:574-91 .

Issa, N.P., Trepel, C. & Stryker, M.P. (2000) Spatial frequency maps in cat visual cortex. J. Neurosci, 20:8504–8514.

Issa, N.P., Rosenberg, A. & Husson, T.R. (2008) Models and measurements of functional maps in V1. J Neurophysiol. 99(6):2745-54.

Kalatsky V.A. & Stryker M.P. (2003) New paradigm for optical imaging: temporally encoded maps of intrinsic signal. Neuron, 38(4):529-45.

Movshon, J.A., Thompson, I.D. & Tolhurst, D.J. (1978) Spatial and temporal contrast sensitivity of neurones in areas 17 and 18 of the cat's visual cortex. J. Physiol. 283:101-20.

Nauhaus, I., Nielsen, K.J., Disney, A.A. & Callaway, E.M. (2012) Orthogonal micro-organization of orientation and spatial frequency in primate primary visual cortex. Nat. Neurosci., 15(12): 1683-90.

Ohki K., Matsuda Y., Ajima A., Kim D.S. & Tanaka S. (2000) Arrangement of orientation pinwheel centers around area 17/18 transition zone in cat visual cortex. Cereb Cortex, 10:593– 601.

Ohki, K., Chung, S., Kara, P., Hubener, M., Bonhoeffer, T. & Reid, R.C. (2006) Highly ordered arrangement of single neurons in orientation pinwheels. Nature 442:925–928.

Petitot J. (2008) Neurogéométrie de la vision, Ecole Polytechnique Editions. 419p.

Ribot J., Tanaka S., Tanaka H., Ajima A. (2006) Online analysis method for intrinsic signal optical imaging. J. Neurosci. Methods 153:8 –20.

Ribot, J., Aushana, Y., Bui-Quoc, E. & Milleret, C. (2013) Organization and Origin of Spatial Frequency Maps in Cat Visual Cortex. J. Neurosci., 33(33):13326-43.

Romagnoni A., Ribot J., Bennequin D. & Touboul J. (2014) Parsimony, exhaustivity and balanced detection in neocortex. ArXiv.

Schummers, J., Mariño, J. & Sur, M. (2002) Synaptic integration by V1 neurons depends on location within the orientation map. Neuron. 36(5):969-78

Schummers, J., Cronin, B., Wimmer, K., Stimberg, M., Martin, R., Obermayer, K. & Koerding K., Sur M. (2007) Dynamics of orientation tuning in cat v1 neurons depend on location within layers and orientation maps. Front Neurosci. 1(1):145-59.

Sharpee, T.O., Sugihara, H., Kurgansky, A.V., Rebrik, S.P., Stryker, M.P. & Miller, K.D. (2006) Adaptive filtering enhances information transmission in visual cortex. Nature. 439(7079):936-42.

Shoham, D., Hübener, M., Schulze, S., Grinvald, A. & Bonhoeffer, T. (1997) Spatiotemporal frequency domains and their relation to cytochrome oxidase staining in cat visual cortex. Nature 385:529 –533.

Swindale N.V. (1991) Coverage and the design of striate cortex. Biol. Cybern., 65(6) :415-24

Swindale, N.V., Shoham, D., Grinvald, A., Bonhoeffer, T. & Hübener, M. (2000) Visual cortex maps are optimized for uniform coverage. Nat. Neurosci., 3(8): 822-6.

Tani, T., Ribot, J., O'Hashi, K. & Tanaka, S. (2012) Parallel development of orientation maps and spatial frequency selectivity in cat visual cortex. Eur. J. Neurosci, 35:44 – 55.

Webster, M.A. & De Valois, R.L. (1985) Relationship between spatial-frequency and orientation tuning of striate-cortex. J Opt Soc Am A 2 :1124-1132

Yokoo T., Knight B.W. & Sirovich L. (2001) An optimization approach to signal extraction from noisy multivariate data. Neuroimage 14:1309 –1326.

Yousef, T., Tóth, E., Rausch, M., Eysel, U.T. & Kisvárday, Z.F. (2001) Topography of orientation centre connections in the primary visual cortex of the cat. Neuroreport. 12(8):1693-9.

Yu, H., Farley, B.J., Jin D.Z. & Sur, M. (2005) The coordinated mapping of visual space and response features in visual cortex. Neuron, 47(2):267-80.

ACKNOWLEDGMENTS

We thank Timothé Coulais for animal care and Sidney Wiener for discussions and comments on the manuscript.

FINANCIAL DISCLOSURE

The research was supported by the Fondation Louis D and the Luz Optique Group (to CM and JR), Rétina France (to CM), the European Community (Marie Curie International Reintegrating Grant), the Foundation Berthe Foussier (to JR) and the CNRS PEPS PTI Program (NeuroGauge Project to AR and JT). The funders had no role in study design, data collection and analysis, decision to publish, or preparation of the manuscript.

AUTHOR CONTRIBUTIONS

J.R. designed and performed experiments, analyzed experimental data and wrote the paper. A.R. analyzed experimental data, designed the model and wrote the paper. C.M. provided administrative and financial support for the experiments, designed and built the experimental post. D.B. and J.T. designed the model, supervised the project and wrote the paper.

FIGURE LEGENDS

Figure 1. SF maps form dipoles at OR PCs. (A) OR map. Four PCs are selected (circles). Dashed line indicates the A17/A18 border. P: Posterior; A: Anterior; L: Lateral; M: Medial. (B) Corresponding SF map. Black pixels correspond to regions where SF preference cannot be estimated accurately with intrinsic optical imaging. Color map in logarithmic scale. (C) Maximal intensity maps around PC 1 for thirty SFs. Note the progression of the response from lateral to medial with increasing SF. (D) Zoom on the SF map for the four PCs circled in (A) and (B). An additional Gaussian low-pass filter with 35 μm sd was used to smooth the data and draw iso-SF lines (black). Logarithmic color map.

Figure 2. A majority of PCs have a SF maximum and a SF minimum in their neighborhood. (A) OR map in A18. Two PCs are selected (red circles). (B) and (C) SF map. The black circle corresponds to a SF hypercolumn centered on PC 1 and 2, respectively. (D) and (E) Top panels: SF distribution close to the PCs 1 and 2, respectively (red circle in (A), (B) and (C)). Bottom panels: SF distribution within a hypercolumn centered on PCs 1 and 2, respectively (black circle in (B) and (C)). (E) and (F) Distribution of PCs with both a SF maximum and a SF minimum, or with only one extremum in A17 and A18, respectively.

Figure 3. Abrupt change in SF representation at PCs with multi-unit recordings. (A) OR map with four electrode penetrations (white dots) performed around a PC (black arrow). (B) Difference between maximal intensity maps induced for stimulus SF of 0.15 cpd and 0.68 cpd. Domains in yellow-white elicit a larger response for 0.15 cpd, those in red-black for 0.68 cpd. The PC falls at the border between two patches. (C) Polar plots of firing rate (Hz) induced by the presentation of eight ORs for these four penetrations. Arrows indicate the

direction of movement of the stimuli. The maximum spike rate is indicated in the bottom right corner. (D) Corresponding SF response curves for stimuli at the preferred OR. X-axis scale is logarithmic. Thin gray lines are normalized firing rate at five depths in superficial layers separated by 100 μm. Minimum and maximum depths are shown at upper right. Thick black line is total normalized spike rate across depths. The zero baseline corresponds to spontaneous activity.

Figure 4. Neurogeometrical model of the pinwheel-dipole around PCs (A) Representation of a complex coordinate $z = r.\exp(i.\varphi)$. (B) Model of the OR PC (iso-OR lines in black). (C) Model of the SF dipole, with parameters equal to the average values across all fits (see Fig. 6). (D) to (F) Modifications of the dipolar architecture shown in (C) when varying the parameters ψ, γ, h_0 and A in Equation (3).

Figure 5. Fit of the SF representation around PCs with the dipolar model. (A-B) Maps of preferred OR and SF respectively. Scale bar: 1 mm. OR pinwheels indicated by the white and gray filled black circles. Gray PCs (not fitted) correspond to those whose SF map either have only one extremum or the indeterminacy region covers more than 75% of the 150 μm circle. (C) Fits of the SF representation of the 18 PCs (white dots in (A) and (B)) with the dipolar model in Equation (3). The least-square errors fits are shown in the lower rows and experimental data in the upper row. They are displayed with decreasing coefficient of determination (R^2) order following linear regression between modeled and experimental data. Note that R^2 can be negative, as the linear regression performed in Matlab® (function *regress*) was done without any DC component (the DC component h_0 in equation (3) was optimized beforehand). (D) Distribution of R^2 among the 186 PCs tested.

Figure 6. Statistics of the fits. Only those fits with $R^2 > 0.8$ were kept. (A) Estimate of the difference between ν_{max} and ν_{min}. This difference is plotted with respect to the percentage of the surface of SF indeterminacy within 150 μm. Linear regression is shown in grey. (B) Scatter plot of h_0 with respect to $(\nu_{max}+\nu_{min})/2$. Linear regression is shown in grey. (C) Distribution of the angle between the maximum and the minimum (estimated from the γ parameter) with respect to the PC. The peak at 180 degrees shows that extrema tends to be aligned with the PC. (D). Distribution of ψ. (E) Scatter plot of A with respect to $(\nu_{max}-\nu_{min})/2$. Linear regression is shown in grey.

SUPPORTING INFORMATION

Figure S1. Maximal intensity maps for the animal shown in Fig. 1. Thirty SFs were presented to the animal. The signal at each pixel that elicited the maximum activation was normalized at 100%. Scale bar: 1 mm.

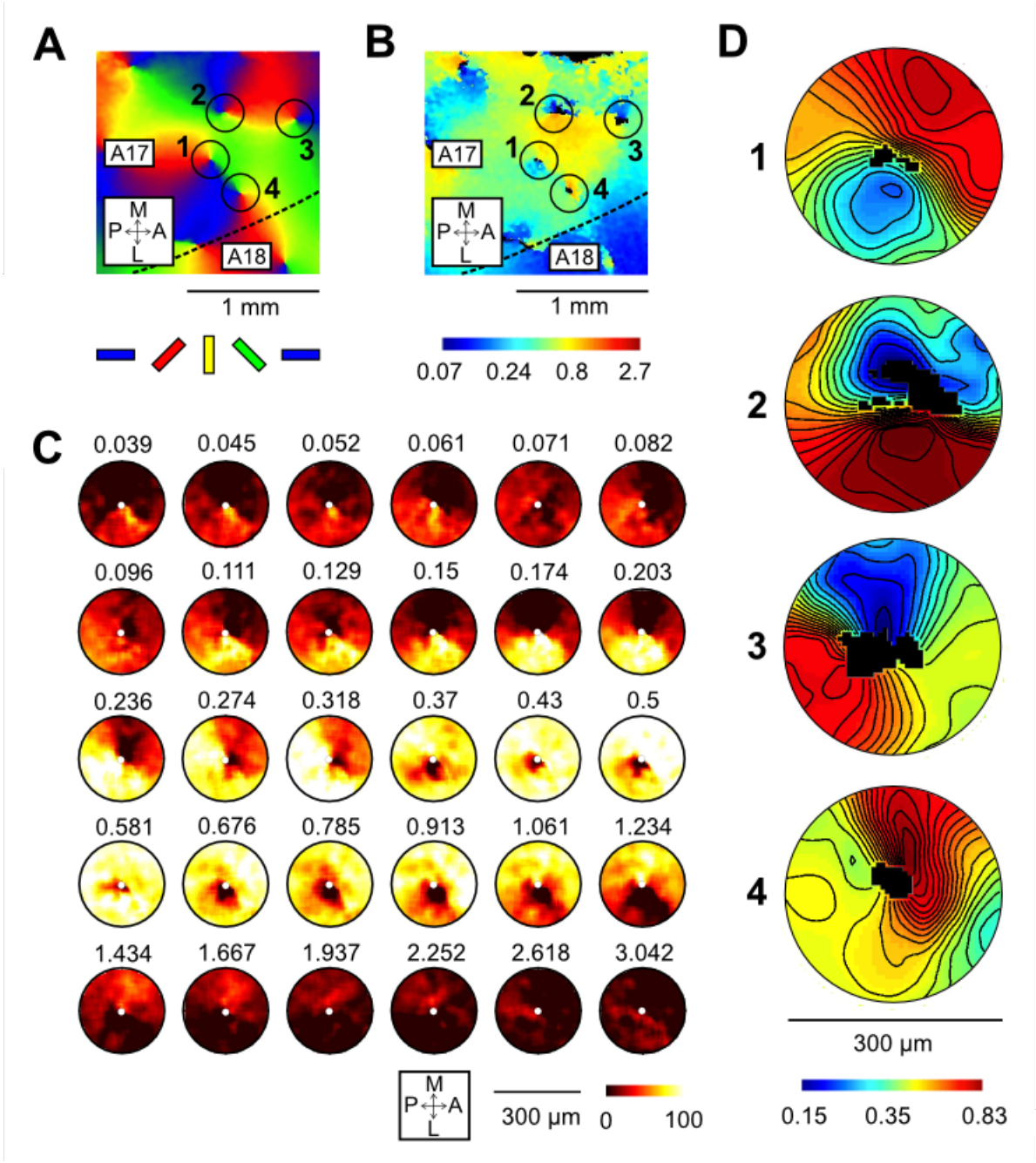

FIGURE 1

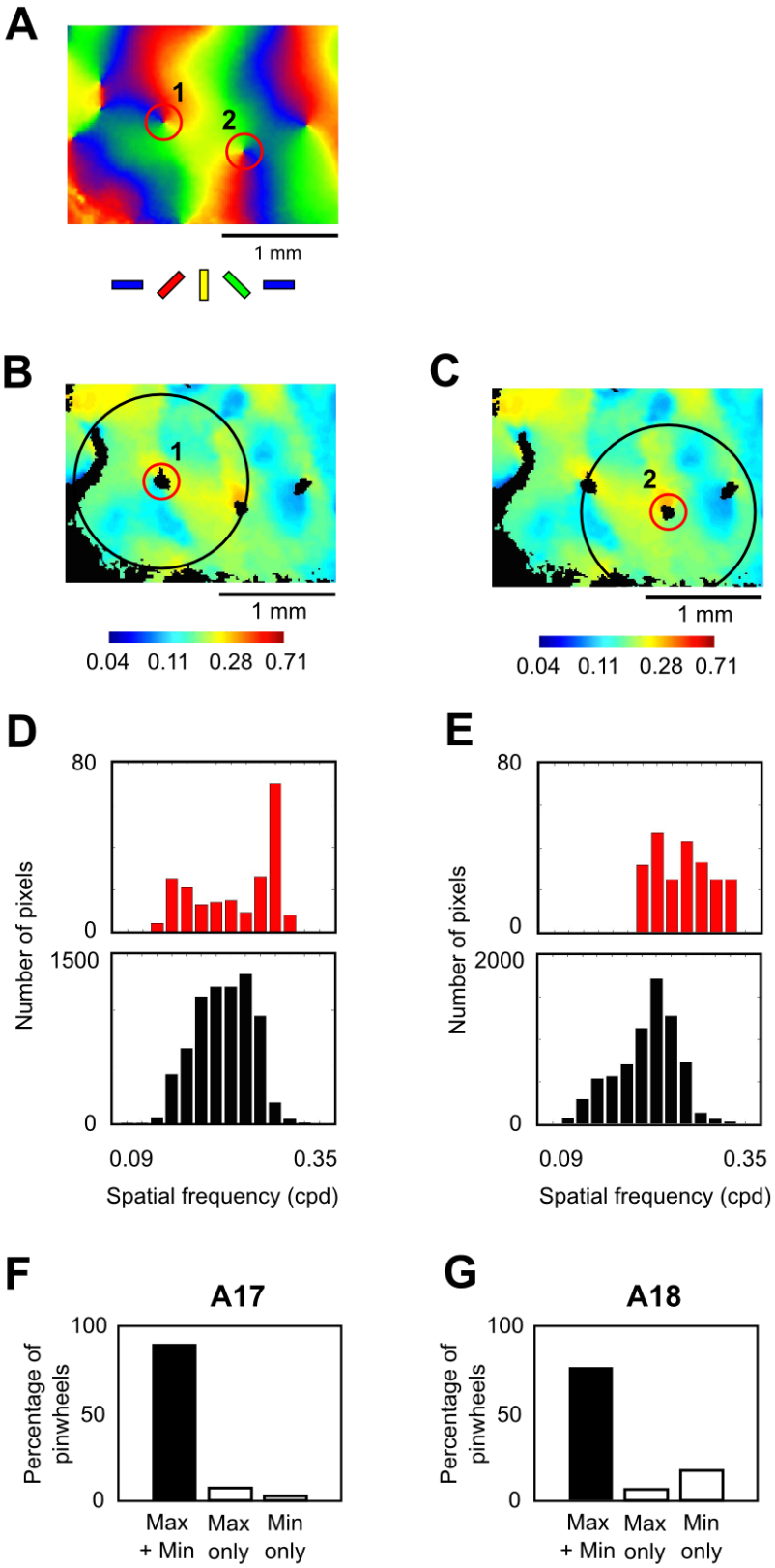

FIGURE 2

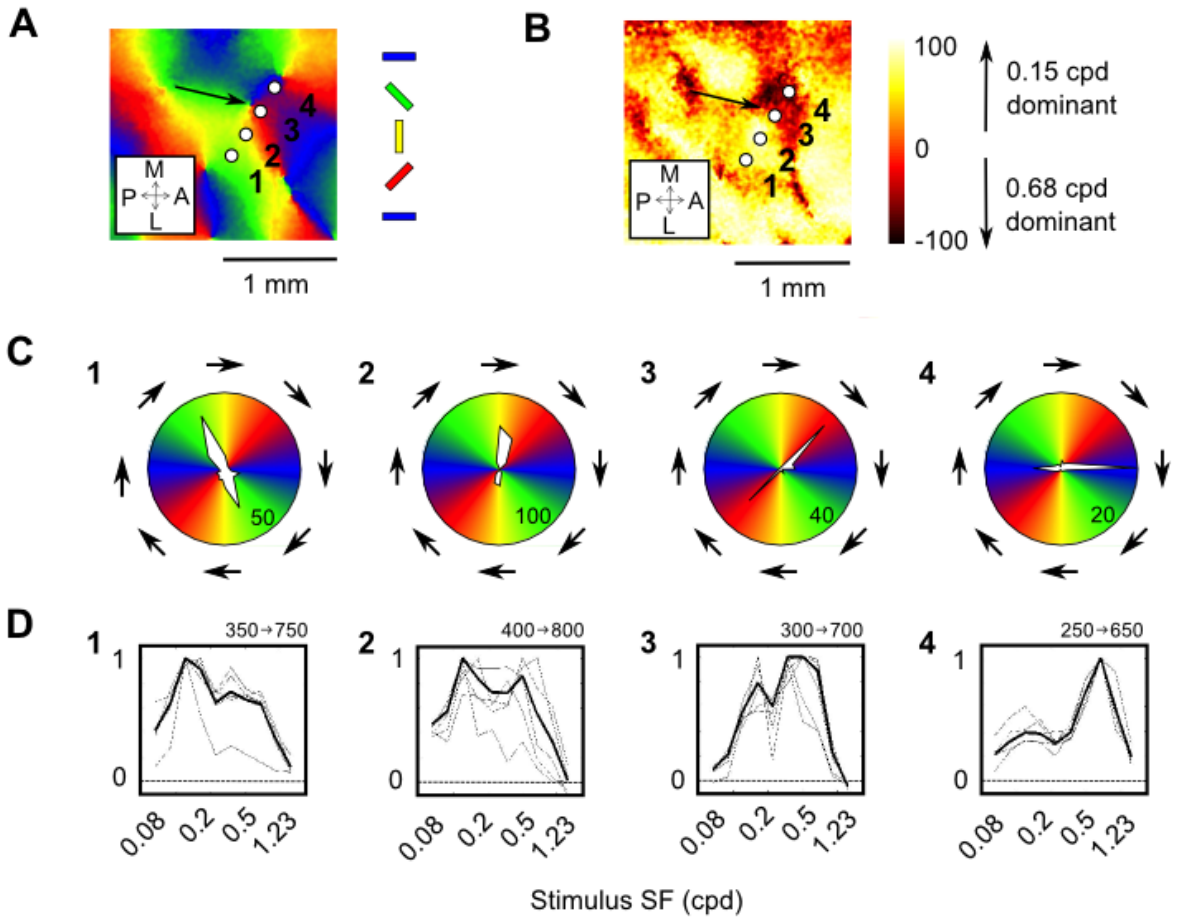

FIGURE 3

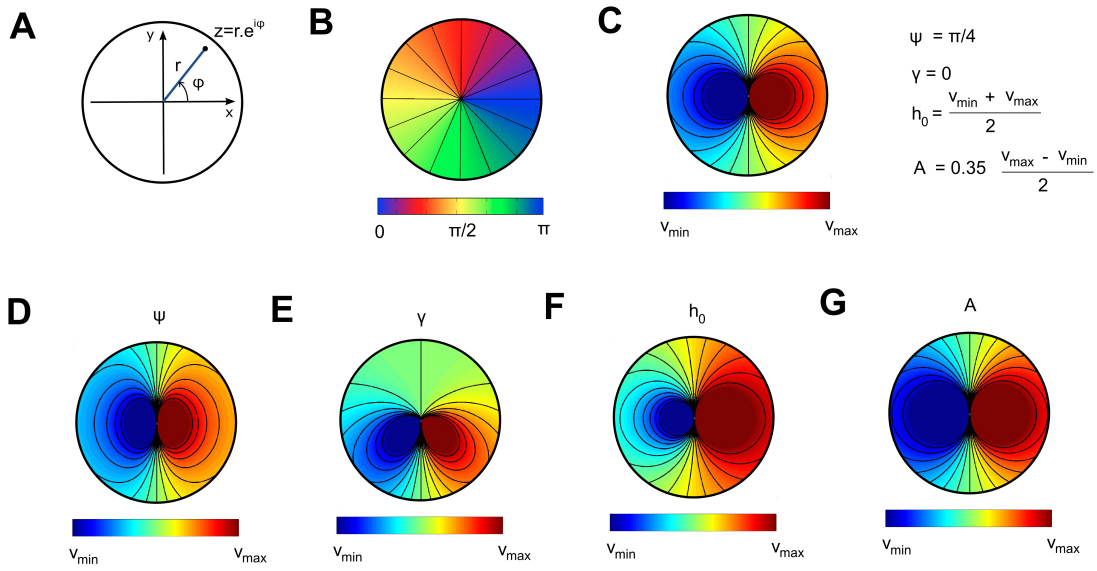

FIGURE 4

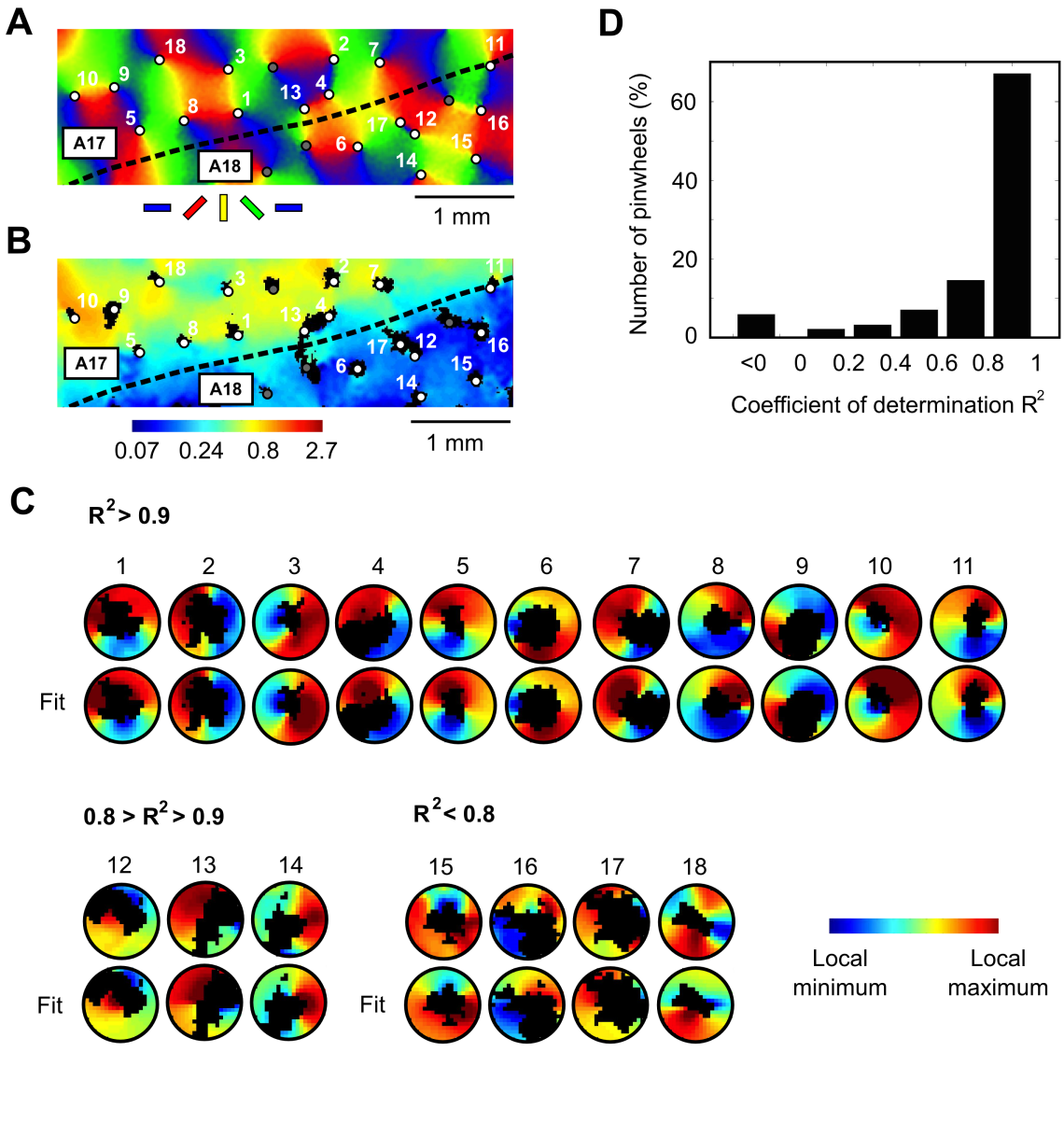

FIGURE 5

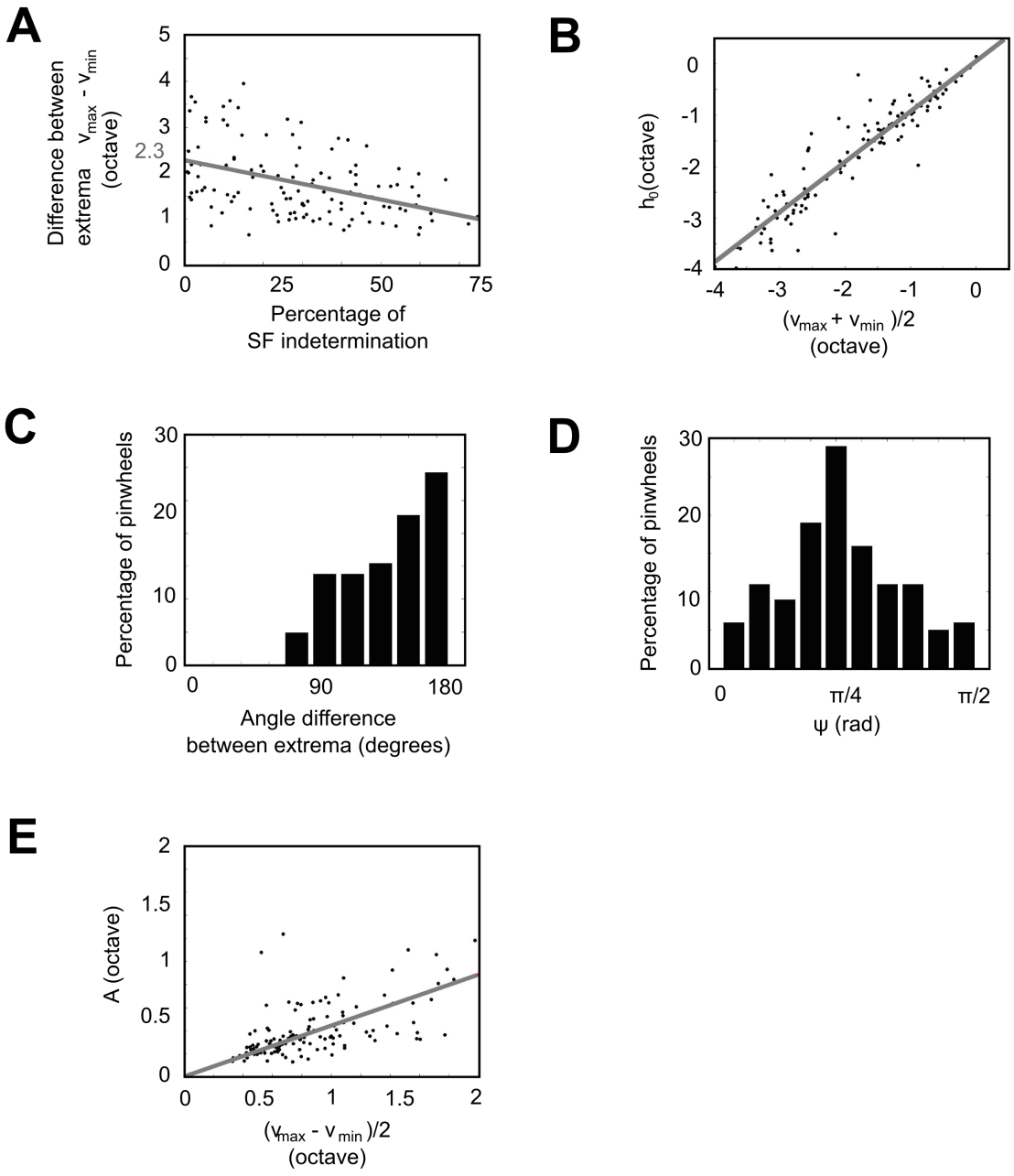

FIGURE 6

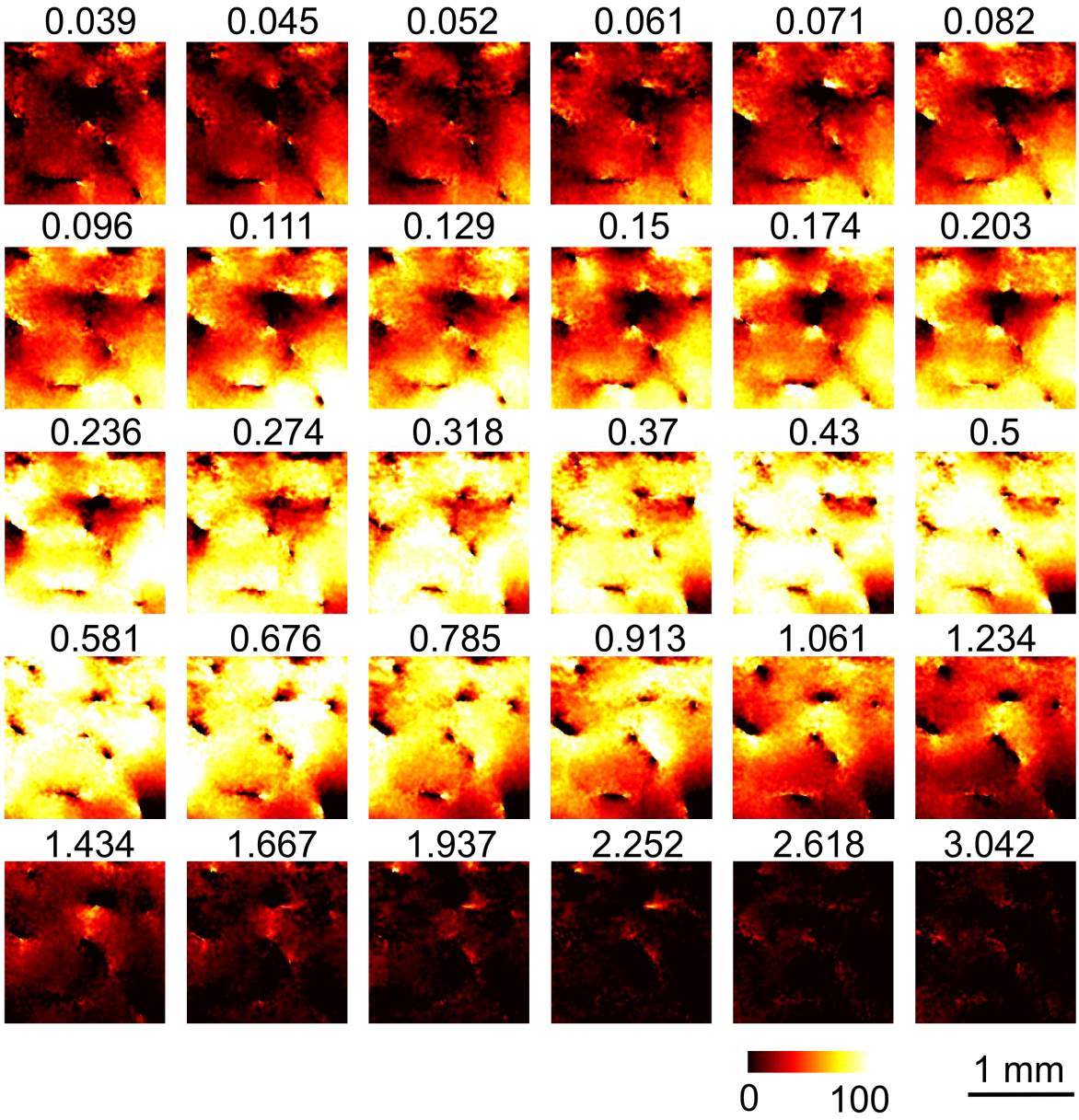

FIGURE S1